Pergamon

Int. J. Heat Mass Transfer. Vol. 38, No. 15, pp. 2833–2841, 1995

0017-9310/95 $9.50+0.00

0017-9310(95)00014-3

Fundamentals of ice making by convection cooling followed by contact melting

J. V. C. VARGAS and A. BEJAN†

Department of Mechanical Engineering and Materials Science, Duke University, Durham, NC 27708-0300, U.S.A.

(*Received* 14 *February* 1994 *and in final form* 10 *December* 1994)

Abstract—In this paper we show that the production of ice by convection cooling followed by contact melting can be maximized by properly selecting the frequency of the intermittent freezing and removal cycle. In the first part of the paper, this principle is illustrated in three configurations: water freezing inside a tube cooled externally by convection, freezing on the outside of a tube cooled internally by convection, and freezing on a plane wall with convection cooling on the back side. The proper dimensionless groups are identified, and the optimal regime of intermittent operation is reported in dimensionless charts. The second part of the paper focuses on the contact melting process that occurs during the gravitational removal of the ice piece. This time-dependent process is the result of the coupling between the thin-film fluid mechanics, the acceleration of the ice piece and the variable length of the direct contact region. The ice fall time predicted by the contact melting analysis was validated by experiments with ice columns falling from vertical tubes heated from the side.

1. INTRODUCTION

The large-scale production of ice continues to be an important engineering objective, because, in addition to the traditional applications (food processing and storage), the repeated freezing and melting of ice is an attractive method of exergy storage [1] (called "the ice harvesting method") and seawater desalination [2]. Two of the most common methods of ice manufacturing are the ice in tube method (Fig. 1), and the ice on tube method (Fig. 6).

In this paper we describe the most fundamental heat transfer features of these ice manufacturing processes. The first objective is to show how the frequency of the intermittent freezing and ice removal cycle can be selected such that the time-averaged production of ice is maximized. This manufacturing optimization principle is applicable to the production of other solid materials, not just ice. The second objective is to construct an analysis of the time-dependent contact melting process that occurs during the gravitational fall of each ice piece. The third objective is to test in the laboratory the predictions made based on the contact melting analysis.

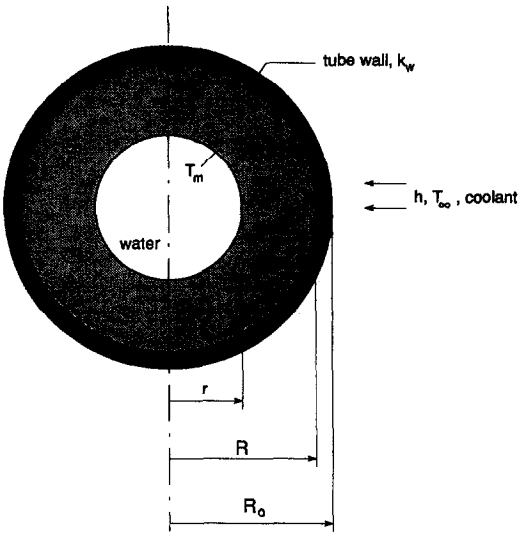

Fig. 1. The freezing of water inside a round tube cooled externally.

2. FREEZING INSIDE A TUBE COOLED EXTERNALLY BY CONVECTION

Consider the configuration sketched in Fig. 1, in which ice forms on the inner side of a cylindrical wall cooled on the outside by convection. In the beginning, the cylinder is filled with water at the freezing point, T_m. The outer wall of the cylinder is exposed to a coolant ($T_\infty < T_m$) when $t > 0$. The heat transfer coefficient between the wall and the coolant, h, is assumed constant. The water movement can be neglected because the buoyancy effect is zero (the liquid is isothermal at T_m). The heat transfer through the ice shell and the tube wall are by quasi-steady conduction, which occurs when the ice Stefan number is small [3].

The relation between the inner radius of the ice annulus (r) and time (t) is obtained by writing that the conduction and convection heat transfer rate from

† Author to whom correspondence should be addressed.

NOMENCLATURE

A	cross-sectional area
$\tilde{A}$	cross-sectional area
b	thickness of tube wall
B	dimensionless group, equation (29)
Bi	generalized Biot number, equation (5)
$\tilde{Bi}$	generalized Biot number, equation (20)
c	specific heat of liquid water
C	dimensionless group, equation (15)
D	diameter of ice sample
g_z	gravitational acceleration in the z direction, Fig. 10
G	dimensionless group, equation (30)
h	heat transfer coefficient
h_{sf}	latent heat of melting
H	length of ice column
k	water thermal conductivity
k_i	ice thermal conductivity
k_w	wall thermal conductivity
m	mass of ice column
p	wetted perimeter of ice column
r	radial position, Figs. 1 and 6
R	inner radius of round tube, Figs. 1 and 6
R_0	outer radius of round tube, Figs. 1 and 6
Ra	Rayleigh number
t	time
t_c	time to steady conduction
t_f	ice fall time
t_{nc}	time to steady natural convection
t_1	time of ice formation
t_2	time of ice removal
T_h	temperature of hot fluid, Fig. 10
T_m	melting point
T_∞	temperature of cold fluid, Figs. 1 and 6
x	dimensionless radial position, r/R
y	dimensionless radial position, r/R_0
z	longitudinal ice travel during removal, Fig. 10.

Greek symbols

α	thermal diffusivity of air
α_{Cu}	thermal diffusivity of copper
β	dimensionless time, equation (27)
β_f	dimensionless ice fall time, equation (31)
δ	ice layer thickness on plane wall
$\tilde{\delta}$	dimensionless ice thickness, equation (14)
Δ_w	thickness of plane wall
ΔT	wall-ambient temperature difference
ζ	dimensionless ice travel, z/H
θ	relative freezing time, equation (10)
λ	thickness of thin water film, Fig. 10
$\tilde{\lambda}$	dimensionless film thickness, equation (28)
μ	water viscosity
ρ	density of ice or water
τ	dimensionless time, equation (4)
$\tilde{\tau}$	dimensionless time, equation (19)
τ_0	time when the tube cross-section fills with ice, equation (6)
$\tau_1, \tilde{\tau}_1$	time of ice formation
$\tau_2, \tilde{\tau}_2$	time of ice removal.

T_m to T_∞ is matched by the rate of freezing at the $r(t)$ interface:

$$(T_m - T_\infty)\left[\frac{\ln(R/r)}{2\pi k_i} + \frac{\ln(R_0/R)}{2\pi k_w} + \frac{1}{h2\pi R_0}\right]^{-1} = \rho h_{sf}\left(-\frac{dr}{dt}\right)2\pi r. \quad (1)$$

This equation can be integrated from $t = 0$, when $r = R$, to obtain an implicit relation between time and inner ice radius,

$$\tau = \frac{x^2}{2}\ln x - \frac{x^2}{4} - \frac{x^2}{2Bi} + \frac{1}{4} + \frac{1}{2Bi} \quad (2)$$

in which the dimensionless variables are defined by

$$x = \frac{r}{R} \quad (3)$$

$$\tau = \frac{tk_i(T_m - T_\infty)}{\rho h_{sf} R^2} \quad (4)$$

$$Bi = \frac{hR_0}{k_i}\left[1 + \frac{hR_0}{k_w}\ln\left(\frac{R_0}{R}\right)\right]^{-1}. \quad (5)$$

The cylinder cross-section fills with ice when $x = 0$, or cf. equation (2),

$$\tau_0 = \frac{1}{4} + \frac{1}{2Bi}. \quad (6)$$

The newly formed ice column continues to be subcooled as τ increases above τ_0.

Let us assume that the sequence of operations associated with removing the ice column lasts t_2 seconds, which in dimensionless terms corresponds to the constant

$$\tau_2 = \frac{t_2 k_i(T_m - T_\infty)}{\rho h_{sf} R^2}. \quad (7)$$

The question we address first is how long should the ice forming process be allowed to run, so that the time-averaged rate of ice production is maximum? Let

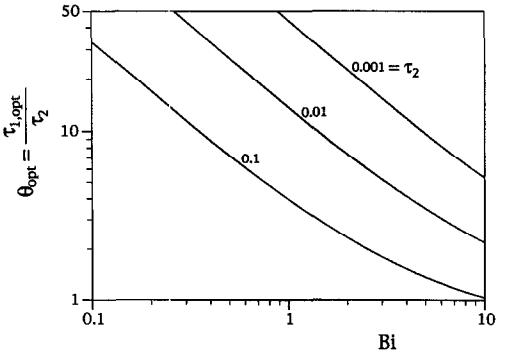

Fig. 2. The optimal freezing time ratio θ_{opt} as a function of the ice-removal time and the Biot number (freezing inside tube).

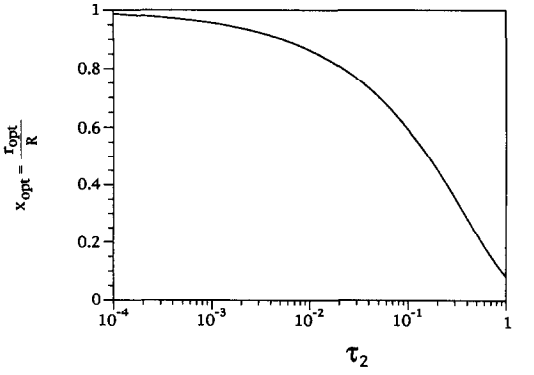

Fig. 3. The optimal inner radius of the ice shell just before removal, as a function of the time of removal (freezing inside tube).

t_1 be the unknown duration of the ice forming process described by equation (2). The amount of ice formed at $t = t_1$ is proportional to the annular cross-sectional area

$$A = \pi R^2 - \pi r^2 = \pi R^2(1-x_1^2) \tag{8}$$

where $x_1 = x(\tau_1)$. This is the amount produced over the total time interval $t_1 + t_2$, i.e. during one cycle of freezing followed by ice removal. The average rate of ice production is proportional to

$$\frac{A}{\tau_1+\tau_2} = \frac{\pi R^2}{\tau_2} \cdot \frac{1-x_1^2(\theta)}{\theta+1} \tag{9}$$

where θ is the relative freezing interval

$$\theta = \frac{\tau_1}{\tau_2}. \tag{10}$$

The function $x_1(\theta)$ is given by equation (2):

$$\theta \cdot \tau_2 = \frac{x_1^2}{2}\left(\ln x_1 - \frac{1}{2} - \frac{1}{Bi}\right) + \frac{1}{4} + \frac{1}{2Bi}. \tag{11}$$

The right side of equation (9) shows that the average rate of ice production varies as the function $(1-x_1^2)/(\theta+1)$, which depends on θ, τ_2 and Bi. The optimal freezing interval θ_{opt} that maximizes this function was determined numerically and plotted in Fig. 2. The ice removal time constant τ_2 can be expected to be smaller than 1. For example, if $t_2 = 20$ seconds, $T_m - T_\infty = 30°C$, and $R = 2$ cm, the τ_2 value is 0.011.

When the ice removal time τ_2 is fixed, the optimal freezing time decreases as the external heat transfer coefficient (Bi) increases. For example, if $Bi = 1$ and $\tau_2 = 0.1$ the optimal time ratio is $\theta_{opt} = 3.96$, which means that the freezing interval should last approximately four times longer than the ice removal interval.

The optimal inner radius of the final ice annulus, $x_{opt} = x(\theta_{opt})$, is only a function of τ_2, and is shown in Fig. 3. The results of Figs. 2 and 3 are valid when the ice front does not reach the centerline of the cylinder, i.e. when $\tau < \tau_0$, or $\theta < \tau_0/\tau_2$. In the preceding numerical example ($Bi = 1$, $\tau_2 = 0.1$), the optimal final inner radius of the ice annulus is $x_{opt} = 0.592$, or $r_{opt} = 0.592R$.

An alternative to the $\theta_{opt}(Bi, \tau_2)$ function of Fig. 2 is the optimal freezing time $\tau_{1,opt}(Bi, \tau_2)$ shown in Fig. 4. This is obtained by multiplying the ordinate of Fig. 2 by τ_2, because $\tau_{1,opt} = \theta_{opt}\tau_2$. Figure 4 shows that the optimal freezing interval $\tau_{1,opt}$ decreases when the ice removal time τ_2 decreases at constant Bi.

To summarize, the ice production cycle is described by the time of ice formation τ_1, followed by the time of ice removal τ_2. The physical impact of the cycle optimization procedure is to maximize the rate of ice production averaged over time.

3. FREEZING ON A PLANE WALL COOLED BY CONVECTION ON THE BACK SIDE

The results developed in the preceding section reach a particularly simple form in the limit in which the tube radius R is sufficiently large that the ice layer is always thin relative to R. In this limit the convection-driven freezing process is the same as on a plane wall of thickness Δ_w and thermal conductivity k_w, with an ice layer of instantaneous thickness δ. The connection between this geometry and the $R \gg (R_0 - R)$ limit of Fig. 1 is represented by $\Delta_w = R_0 - R$ and $\delta = R - r$.

Since the analysis follows the steps presented in Section 2, we omit the analytical details and list only

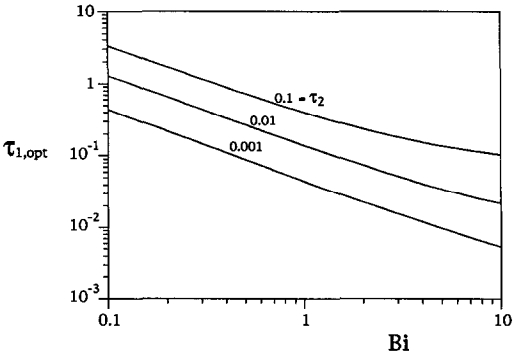

Fig. 4. The optimal freezing time $\tau_{1,opt}$ as a function of the ice-removal time and the Biot number (freezing inside tube).

the results. In place of equation (2) we obtain the implicit function $\delta(t)$ given by

$$\frac{t}{\rho h_{sf}}(T_m - T_\infty) = \frac{\delta^2}{2k_i} + \delta\left(\frac{\Delta_w}{k_w} + \frac{1}{h}\right). \quad (12)$$

This can be nondimensionalized as the function $\tilde{\delta}(\theta)$.

$$\theta = \tfrac{1}{2}\tilde{\delta}^2 + C\tilde{\delta} \quad (13)$$

by using the notation $\theta = t_1/t_2$, equation (10) and

$$\tilde{\delta} = \delta\left[\frac{\rho h_{sf}}{t_2 k_i (T_m - T_\infty)}\right]^{1/2} \quad (14)$$

$$C = \left(\frac{\Delta_w}{k_w} + \frac{1}{h}\right)\left[\frac{\rho h_{sf} k_i}{t_2 (T_m - T_\infty)}\right]^{1/2}. \quad (15)$$

The problem of determining the optimal freezing time t_1 (or θ_1) reduces to maximizing the function $\tilde{\delta}(\theta)/(\theta+1)$ with respect to θ. The result is given by

$$\theta_{opt} = 1 + 2^{1/2} C \quad (16)$$

which is illustrated in Fig. 5. The optimal freezing time increases monotonically as the C constant increases.

Noteworthy is the limit $C = 0$ in which $\theta_{opt} = 1$. This limit means that when the thermal resistance between the water (T_m) and the coolant (T_∞) is dominated by the ice layer, the optimal freezing time equals the time required to remove the ice layer. In the opposite limit, $C \to \infty$, the optimal freezing time behaves as $\theta_{opt} = 2^{1/2}C$. Note finally that the present results have a simpler form than in Section 2, because in Fig. 5 θ_{opt} is a function of a single parameter (C). The corresponding θ_{opt} results for freezing inside a tube (Fig. 2) depend on two independent parameters (τ_2, Bi).

4. FREEZING ON THE OUTSIDE OF A TUBE COOLED INTERNALLY BY CONVECTION

The production of ice on the outside of a tube cooled internally by convection can be maximized by applying the method of Section 2 to the geometry

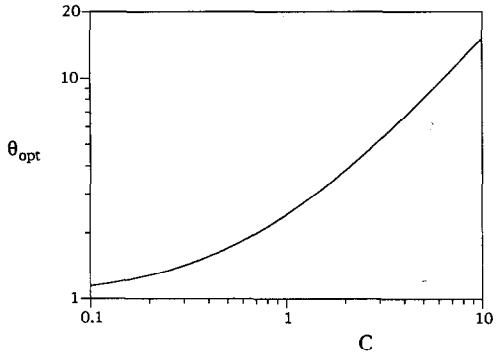

Fig. 5. The optimal freezing time ratio θ_{opt} when the ice layer is formed on a plane wall.

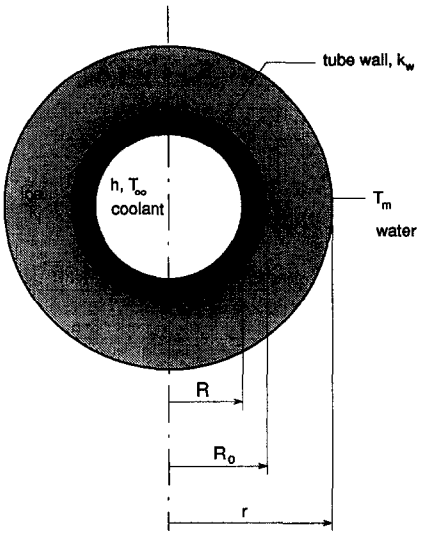

Fig. 6. The freezing of water on the outside of a tube cooled internally.

presented in Fig. 6. We skip the analytical details and report that the position of the freezing front is now given by

$$\tilde{\tau} = \frac{y^2}{2}\ln y - \frac{y^2}{4} + \frac{y^2}{2\tilde{Bi}} + \frac{1}{4} - \frac{1}{2\tilde{Bi}} \quad (17)$$

where

$$y = \frac{r}{R_0} \quad (18)$$

$$\tilde{\tau} = \frac{t k_i (T_m - T_\infty)}{\rho h_{sf} R_0^2} \quad (19)$$

$$\tilde{Bi} = \frac{hR}{k_i}\left[1 + \frac{hR}{k_w}\ln\left(\frac{R_0}{R}\right)\right]^{-1}. \quad (20)$$

At the end of the freezing time interval t_1, the cross sectional area of the ice annulus is $\tilde{A} = \pi R_0^2 (y_1^2 - 1)$, where $y_1 = y(\tilde{\tau}_1)$ in accordance with equation (17). The average rate of ice production is

$$\frac{\tilde{A}}{\tilde{\tau}_1 + \tilde{\tau}_2} = \frac{\pi R_0^2}{\tilde{\tau}_2} \cdot \frac{y_1^2(\theta) - 1}{\theta + 1} \quad (21)$$

where θ is the relative freezing time, $\theta = t_1/t_2 = \tilde{\tau}_1/\tilde{\tau}_2$, and the function $y_1(\theta)$ is given by equation (17):

$$\theta \cdot \tilde{\tau}_2 = \frac{y_1^2}{2}\left(\ln y_1 - \frac{1}{2} + \frac{1}{\tilde{Bi}}\right) + \frac{1}{4} - \frac{1}{2\tilde{Bi}}. \quad (22)$$

The function $(y_1^2 - 1)/(\theta + 1)$ identified in equation (21) was maximized numerically, and the results are reported in Figs. 7–9. The trends are similar to those seen in Figs. 2–4 for freezing inside tubes. These similarities are enhanced by the fact that the dimensionless groups employed in this section (y, $\tilde{\tau}$, $\tilde{Bi}$) were carefully selected to be the analogs of the groups (x, τ, Bi) employed in Section 2. The limit where the optimal thickness of the ice shell is small relative to R_0 is

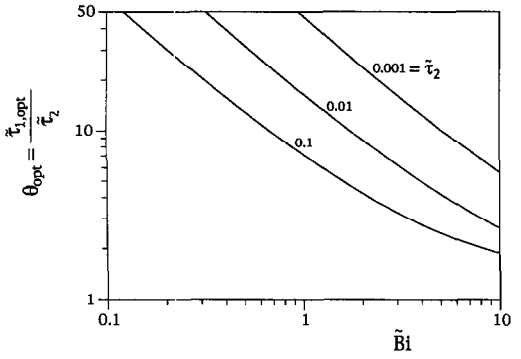

Fig. 7. The optimal freezing time ratio θ_{opt} for freezing on the outside of a tube.

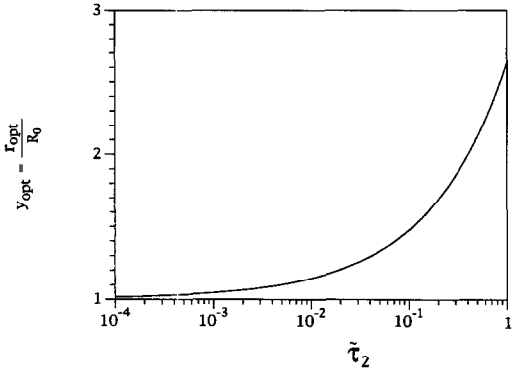

Fig. 8. The optimal outer radius of the ice shell formed on the outside of a tube.

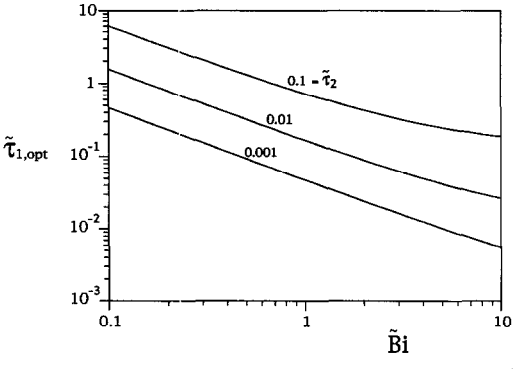

Fig. 9. The optimal freezing time $\tilde{\tau}_{1,opt}$ for freezing on the outside of a tube.

covered by the "ice on plane wall" results reported in the preceding section.

To summarize, when the ice is made inside a vertical tube, τ_1 is the time of the solidification process, and τ_0 the time when the ice front reaches the centerline. When $\tau_1 < \tau_0$, the produced ice is a cylindrical tube, and when $\tau_1 > \tau_0$ it is a subcooled rod. The present optimization results are valid for $\tau_1 < \tau_0$, because the objective is to produce a maximum amount of solid (ice), not subcooled solid.

5. CONTACT MELTING AND FALL OF THE PIECE OF ICE

A new and interesting contact melting phenomenon occurs during the fall of the ice piece from the wall on which it was made. As shown in Fig. 10, the ice can be removed by gravity while heating the wall convectively (h, T_h) starting at $t = 0$. The ice piece slides downward while rubbing against a film of water. The time until the ice leaves completely the wall surface can be anticipated based on *contact melting theory* [4]. Although Fig. 10 shows the removal of the ice formed inside a tube, the results reported in this section apply to ice formed on vertical walls of any shape, e.g. on the outside of tubes, or on plane walls.

The contact melting phenomenon of Fig. 10 is new relative to the current state of contact melting heat transfer research, which was reviewed recently [4]. In brief, the published studies dealt with melting inside heated capsules [5–10], and the movement of heated bodies through solid phase-change media [11, 12]. The melting heat transfer along plane surfaces with relative motion was studied as well [13].

The thin-film assumptions on which contact melting analyses are based are well documented (see, for example, Roy and Sengupta [8]), and are not repeated here. To these we add two more simplifying assumptions:

(a) The water Stefan number is small, $c(T_h - T_m)/h_{sf} \ll 1$, such that the temperature distribution across the melt water film thickness λ is linear.

(b) The wall is thin and conductive enough such that the transient conduction effect in the wall can be neglected. The heat transfer through the wall is quasisteady because the temperature of the inner and outer surfaces of the wall vary as the melt film thickness increases from $\lambda = 0$ at $t = 0$.

Assumption (b) allows us to express the instantaneous heat flux from the heat source (T_h) to the ice (T_m) as

$$\rho h_{sf} \frac{d\lambda}{dt} = (T_h - T_m)\left[\frac{\lambda}{k} + \frac{\ln(R_0/R)}{2\pi k_w} + \frac{1}{2\pi R_0 h}\right]^{-1}. \tag{23}$$

The downward travel of the ice $z(t)$ is governed by Newton's second law of motion,

$$m\frac{d^2z}{dt^2} = mg_z - (H - z)p\frac{\mu}{\lambda}\frac{dz}{dt} \tag{24}$$

in which m is the mass of the piece of ice, and p is the wetted perimeter of the contact melting surface (e.g. $p = 2\ \pi\ R$ inside a round tube). By using m and p (instead of R, T_0, H) in the analysis, we extend the applicability of this analysis to the contact-melting removal of ice columns of any cross-section, and to ice shells that form on the outside of vertical walls of any shape. In equation (24) it is assumed that m is a

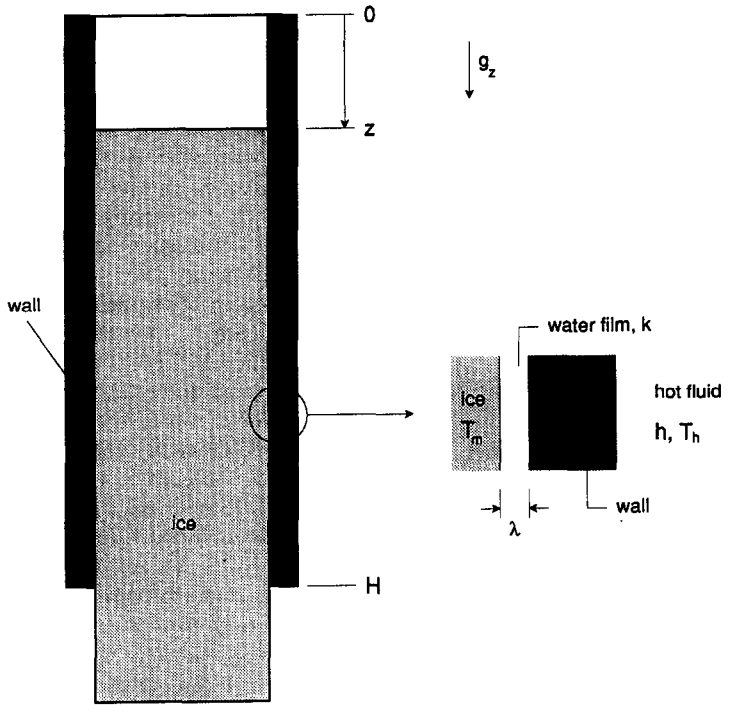

Fig. 10. The removal of the piece of ice by heating the wall.

constant during the ice removal process, or that the thin-film melting process does not erode significantly the piece of ice. The last term in equation (24) accounts for the total friction force due to Couette flow in the melt film, where $(H-z)p$ is the instantaneous contact area.

Integrated in time, equations (23) and (24) deliver the film thickness $\lambda(t)$ and vertical position of the falling ice $z(t)$. We performed this operation numerically, by nondimensionalizing equation (23) (integrated in time) and equation (24) as

$$\beta = \tilde{\lambda}^2 + G\tilde{\lambda} \tag{25}$$

$$\frac{d^2\zeta}{d\beta^2} = 1-(1-\zeta)\frac{B}{\tilde{\lambda}}\frac{d\zeta}{d\beta} \tag{26}$$

where

$$\beta = t\left(\frac{g_z}{H}\right)^{1/2} \quad \zeta = \frac{z}{H} \tag{27}$$

$$\tilde{\lambda} = \lambda\left(\frac{g_z}{H}\right)^{1/4}\left[\frac{\rho h_{sf}}{2k(T_h-T_m)}\right]^{1/2} \tag{28}$$

$$B = \frac{\mu pH}{m}\left[\frac{\rho h_{sf}}{2k(T_h-T_m)}\right]^{1/2} \tag{29}$$

$$G = \left[\frac{\ln(R_0/R)}{2\pi k_w} + \frac{1}{2\pi R_0 h}\right]\left[\frac{2k\rho h_{sf}}{(T_h-T_m)(H/g_z)^{1/2}}\right]^{1/2}. \tag{30}$$

Equations (25) and (26) were integrated starting from $\zeta = d\zeta/d\beta = 0$ at $\beta = 0$. Equation (26) was integrated using a Runge–Kutta method of 4th–5th order with controlled step size, while keeping the local truncation error below a prescribed tolerance of 10^{-6} [14]. Equation (25) shows that $\beta = 0$ represents a singularity point in equation (26). This singularity was avoided by starting the integration from $\beta = 10^{-4}$ where both ζ and $d\zeta/d\beta$ are approximately zero. Since in the beginning the $\zeta(\beta)$ curve is very flat, numerical stability required the use of sufficiently small step size that was adjusted according to the local truncation error. In this way the solution was generated using little computational time.

The calculated ice travel history is illustrated in Fig. 11 for $G = 10^4$, which is the G order of magnitude relevant to the experiments described in the next section. The piece of ice starts its travel extremely slowly, and accelerates its fall dramatically after it executes about 20% of its total travel. The time when the trailing end of the falling ice leaves the tube is the β value marked by the $\zeta(\beta)$ curve on the abscissa of Fig. 11. In other words, the ice fall time β_f is defined by

$$\zeta(\beta_f) = 1 \tag{31}$$

and the β_f (B, G) curves that emerge are reported in Fig. 12. The ice fall time increases monotonically with the dimensionless group B, i.e. as the contact area pH increases, or as the driving temperature difference decreases. This time increases also as the thermal resistance (G) associated with the wall and the external flow becomes significant. In the B and G range covered by Fig. 12, the numerical β_f values displayed

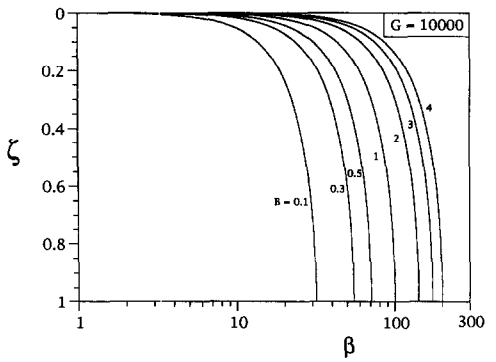

Fig. 11. The downward travel of the piece of ice removed by contact melting from the side.

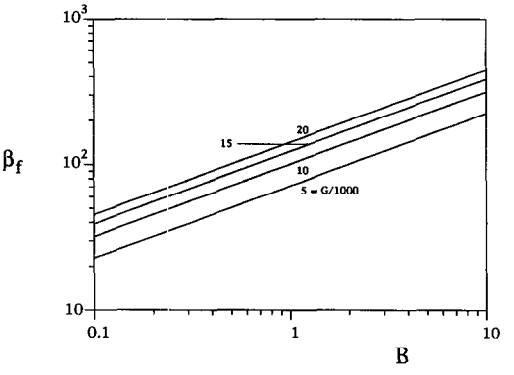

Fig. 12. The time until the ice leaves completely the wall heated from the side.

in the figure are correlated within 5% by the expression

$$\beta_f = 0.35G^{0.61}B^{0.5}. \quad (32)$$

It is important to note that the ice fall time t_f (or β_f), predicted by contact melting analysis is not the same as the removal time t_2, which was regarded as a constant in Sections 2–4. The time t_2 accounts for a considerably longer series of operations that begins with interrupting the coolant flow, replacing the coolant with a flow heating agent, allowing for an interval longer than t_f to make sure that every single ice piece falls off the heated wall, replacing the heating agent with coolant, and cooling the wall long enough to make the start of the ice making phase (t_1) possible.

6. EXPERIMENTAL MEASUREMENT OF THE ICE FALL TIME

The ice fall time obtained by solving numerically equations (25), (26) and (31) was validated through measurements made in the laboratory. Two ice sample sizes were used in these experiments, Table 1. The procedure consisted of freezing water in a tube (height H, inside diameter D, wall thickness b), bringing the ice sample to the isothermal state near the melting point, and measuring the time until the ice sample fell out of the vertical tube.

Each ice sample was made in a commercial copper tube placed in a freezer at $-8°C$. Two thermocouples were placed at mid-height in the ice sample, one on the centerline, and the other at the surface. Before each contact melting run, the tube (with ice in it) was immersed for approximately 3 h in an insulated container filled with a mixture of crushed ice and water. The ice sample temperature was monitored until the readings of both thermocouples indicated 0°C. At that moment the tube was taken out of the container and suspended vertically in a support in the laboratory atmosphere. This move, which lasted about 1 s, marked the beginning of the contact melting run, $t = 0$.

Ten runs were executed for each of the sample sizes listed in Table 1. The precision limit P_t was calculated as twice the standard deviation exhibited by the set of ice-fall time measurements obtained with one sample size (cf. ref. [15]). The bias limit of the chronometer used in the measurements was ± 0.01 s. The uncertainty for t was calculated using the formula $U_t = (P_t^2 + B_t^2)^{1/2}$.

The outer surface of the tube was heated by natural convection. The h coefficient [needed to estimate G, equation (30)] was calculated based on Lienhard's approximate formula [16]. This approximate estimate was more than adequate because it is not critical to know G very accurately in order to estimate the ice fall time. For example, if $D = 5$ cm, $H = 25$ cm and $b = 1.5$ mm, an error of 30% in the estimation of h leads to an error of 11.5% in the theoretical prediction of the ice fall time based on Fig. 12.

The calculation of h was based on the assumption that the boundary layer natural convection on the outside of the tube is in the steady state. This assumption is justified because the time scale associated with the establishment of steady natural convection is small relative to the duration of the contact melting process. That time scale is $t_{nc} \sim (H^2/\alpha)Ra^{-1/2}$, where Ra is the Rayleigh number based on height and wall-ambient ΔT [17]. For example, when $H = 25$ cm, $\Delta T = 25°C$ and the air properties are evaluated at 12°C, we obtain $t_{nc} \sim 0.4$ s. When the tube is shorter, $H = 8$ cm, the boundary layer reaches steady state after $t_{nc} \sim 2$ s.

The theory tested in these experiments is based also on the assumption that the conduction through the wall of the copper tube is steady. The conduction steady state is achieved after a time of order $t_c \sim b^2/\alpha_{Cu}$, which means that $t_c \sim 0.02$ s when $b = 0.15$ cm, and $t_c \sim 0.01$ s when $b = 0.1$ cm. These time estimates show that during the experiments of Table 1 the conduction through the tube wall was steady.

Table 1 shows that there is good quantitative agreement between the predicted and measured times for the fall of the ice sample. Furthermore, both the predicted and measured times decrease from the first set of runs to the second. The fact that the measured times

Table 1. Comparison between the measured and predicted times of when the ice sample falls out of a vertical tube

						Ice fall times [s]				
H [cm]	D [cm]	b [mm]	B	G	β_f	Predicted	Measured	P_t	B_t	U_t
25	5	1.5	0.54	14000	87.31	13.94	17.83	4.00	0.01	4.00
8	3	1	0.9	13000	118.7	10.72	15.01	4.62	0.01	4.62

are longer than the predicted times can be attributed to a small degree of subcooling that may still be present at the start of the contact melting run, or to the wall roughness of the commercial tubes employed. Another, less likely explanation is that some of the liquid film drains and leaves spotty air gaps, which decrease the heat transfer and cause a slower drop rate.

7. CONCLUSIONS

There are two main ideas in the work we have just reported. First, the production of ice by intermittent freezing can be maximized by selecting the frequency of the freezing and removal cycle. We illustrated this principle in three ice-making configurations: freezing inside a tube with convection cooling on the outside, freezing on the outside of a tube with convection cooling on the inside, and freezing on a plane wall with convection cooling on the back side. This design optimization principle appears to be general, in other words, the time-averaged production of ice can be maximized in other geometric configurations.

The second idea is that when the ice piece is removed gravitationally by heating the wall, the motion is governed by a time dependent contact melting process. The fundamental feature that distinguishes the present contact melting process from the other contact melting cases documented in the literature [4], is that it is time-dependent (not quasisteady). Its evolution is tied to the dynamics of the ice piece and to the time-dependent size of the contact region. This contact melting process is one in a potentially long list of contact melting configurations in which the melting material moves with acceleration (falls) along the heater surface. Examples are the fall of ice from the fins and tubes of the evaporator of a defrosting refrigerator and freezer [18], and, outdoors, from electric cables, tree branches and buildings. This new class of time-dependent contact melting phenomena deserves attention in future studies.

The solidification analyses of equations (1)–(22) are based on the assumption that the conduction proces is quasisteady. As shown in ref. [3] this classical assumption is valid when the ice Stefan number is small, $c_{ice}(T_m - T_\infty)/h_{sf} \ll 1$. It is particularly appropriate for ice making processes, where, for example, $T_m - T_\infty = 8$ K corresponds to $Ste_{ice} = 0.049$. The solidification processes discussed in this paper are to be distinguished from *rapid* solidification processes. The latter are receiving considerable attention (e.g. Kang *et al.* [19]), and are employed in the production of special alloys, where the objective is to generate a fine grain structure in the final product. In spite of the different Stefan number, the idea that the solidification and removal cycle can be optimized for maximum production of solid continues to be valid, and deserves to be applied to rapid solidification processes as well. In such applications the solid Stefan number will appear as an additional group in the nondimensional reporting of the final results.

Acknowledgements—This work was supported by the National Science Foundation and the Conselho Nacional de Desenvolvimento Cientifico e Tecnologico—CNPq (Brasil). Prof. Bejan acknowledges with gratitude the advice received in 1992 and 1993 from Dr J. S. Lim, Senior Research Scientist, Refrigeration and Airconditioning Laboratory, Samsung R&D Center, Suwon, Korea, who drew his attention to the heat transfer phenomena that limit the development of modern refrigerator technology.

REFERENCES

1. A. Bejan, *Entropy Generation through Heat and Fluid Flow*, pp. 169–170. Wiley, New York (1982).
2. A. Martindale, B. R. Parr and M. J. S. Smith, Immiscible refrigerant freeze desalination process operations of bench and pilot scale, *Proceedings of the 3rd International Symposium of Fresh Water from the Sea*, vol. 3, pp. 71–82 (1970).
3. A. Bejan, *Heat Transfer*, p. 188. Wiley, New York. (1993).
4. A. Bejan, Contact melting heat transfer and lubrication, *Adv. Heat Transfer* **24,** 1–38 (1994).
5. D. Nicholas and Y. Bayazitoglu, Heat transfer and melting front within a horizontal cylinder, *J. Solar Energy Engng* **102,** 229–232 (1980).
6. M. Bareiss and H. Beer, An analytical solution of the heat transfer process during melting of an unfixed solid phase change material inside a horizontal tube, *Int. J. Heat Mass Transfer* **27,** 739–746 (1984).
7. A. Prasad and S. Sengupta, Numerical investigation of melting inside a horizontal cylinder including the effects of natural convection, *J. Heat Transfer* **109,** 803–806 (1987).
8. S. K. Roy and S. Sengupta, The melting process within spherical enclosures, *J. Heat Transfer* **109,** 460–462 (1987).
9. P. A. Bahrami and T. G. Wang, Analysis of gravity and conduction-driven melting in a sphere, *J. Heat Transfer* **109,** 806–809 (1987).
10. B. W. Webb, M. K. Moallemi and R. Viskanta, Experiments on melting of unfixed ice in a horizontal cylindrical capsule, *J. Heat Transfer* **109,** 454–459 (1987).
11. S. H. Emerman and D. L. Turcotte, Stokes's problem with melting, *Int. J. Heat Mass Transfer* **26,** 1625–1630 (1983).
12. M. K. Moallemi and R. Viskanta, Melting around a

migrating heat source, *J. Heat Transfer* **107,** 451–458 (1985).
13. A. Bejan, The fundamentals of sliding contact melting and friction, *J. Heat Transfer* **111,** 13–20 (1989).
14. D. Kincaid and W. Cheney, *Numerical Analysis*, chap. 8. Wadsworth, Belmont, CA (1981).
15. Editorial, Journal of Heat Transfer policy on reporting uncertainties in experimental measurements and results, *J. Heat Transfer* **115,** 6 (1993).
16. J. H. Lienhard, On the commonality of equations for natural convection from immersed bodies, *Int. J. Heat Mass Transfer* **16,** 2121–2123 (1973).
17. A. Bejan, *Convection Heat Transfer* (2nd Edn), p. 223. Wiley, New York (1995).
18. J. V. C. Vargas, A. Bejan and A. Dobrovicescu, The melting of an ice shell on a heated horizontal cylinder, *J. Heat Transfer* **116,** 702–708 (1994).
19. B. Kang, Z. Zhao and D. Poulikakos, Solidification of liquid metal droplets impacting sequentially on a solid surface, *J. Heat Transfer* **116,** 436–445 (1994).